Polyhedron 155 (2018) 163–169

Contents lists available at ScienceDirect

Polyhedron

journal homepage: www.elsevier.com/locate/poly

CO_2 adsorption under humid conditions: Self-regulated water content in CAU-10

Valeria B. López-Cervantes [a], Elí Sánchez-González [a,*], Tamara Jurado-Vázquez [a], Adriana Tejeda-Cruz [b], Eduardo González-Zamora [c,*], Ilich A. Ibarra [a,*]

[a] Laboratorio de Fisicoquímica y Reactividad de Superficies (LaFReS), Instituto de Investigaciones en Materiales, Universidad Nacional Autónoma de México, Circuito Exterior s/n, CU, Del. Coyoacán, 04510 Ciudad de México, Mexico
[b] Departamento de Materiales Metálicos y Cerámicos, Instituto de Investigaciones en Materiales, Universidad Nacional Autónoma de México, Circuito Exterior s/n, CU, Del. Coyoacán, 04510 Ciudad de México, Mexico
[c] Departamento de Química, Universidad Autónoma Metropolitana-Iztapalapa, San Rafael Atlixco 186, Col. Vicentina, Iztapalapa, C. P. 09340 Ciudad de México, Mexico

ARTICLE INFO

Article history:
Received 26 May 2018
Accepted 11 August 2018
Available online 21 August 2018

Keywords:
CAU-10
CO_2 adsorption
Water adsorption
Diffusion
Metal–Organic Frameworks

ABSTRACT

The CO_2 capture properties of CAU-10 were investigated at different relative humidity conditions. The total CO_2 capture increased 1.3-fold from 5.4 wt% under anhydrous conditions to 7.3 wt% at 5% RH and 303 K. The hydrophobicity of the pore provides to the material CAU-10 a 'self-regulated' water content, which promoted the enhancement of the CO_2 uptake in the low relative humidity domain (3–20% HR), resulting in a 'constant' uptake in this whole range. Adsorption–desorption cycles experiments on a hydrated sample, confirmed the retention of the CO_2 uptake capacity under humid conditions. CAU-10 showed to be a promising material for CO_2 capture under industrial relevant conditions.

1. Introduction

The accelerated growth of the world population during the last decades has demanded a greater production of energy, this has caused an increase in the combustion of fossil fuels, causing an alarming release of carbon dioxide (CO_2) into the atmosphere. The rate of increase of atmospheric CO_2 over the past 70 years is nearly 100 times larger than that at the end of the last ice age [1]. Globally averaged concentrations for CO_2 reached 403.3 parts per million in 2016, up from 400 ppm in 2015, this represents the largest annual increase in the 50-year world record [2]. A main part of these CO_2 emissions corresponds to the combustion of fossil fuels, which is our principal energy source. Thus, the carbon dioxide capture and sequestration (CCS) in post-combustion effluents has become a great challenge for scientists [3].

The current technology for CCS is the CO_2 absorption in alkanolamine solutions. Although, is an efficient process there are several drawbacks in the use of amines solutions. The regeneration of these solutions is highly energy consuming, making this process not economically viable. A demand for more suitable adsorbents has led to a list of desired properties of this ideal adsorbent [4]. An ideal adsorbent for the post-combustion capture of CO_2 should exhibit: (i) high CO_2 adsorption capacity; (ii) fast adsorption kinetics; (iii) high CO_2 selectivity; (iv) mild regeneration conditions; (v) stability during adsorption–desorption cycling; (vi) stability towards moisture; and (vii) low cost of production. Porous materials are an alternative to fulfill with these needed properties [5].

One of the most promising candidates are Metal–Organic Frameworks (MOFs), a family of porous solids constructed from metal ions and bridging organic ligands that form two or three-dimensional periodic arrays which present great surface areas and size-tunable pores[6–8]. Their CO_2 adsorption capacity is directly tailored as a function of the topology and chemical composition of the pores [9], These points cover the first, second and third criteria. The fourth criteria, the regeneration step, is a key feature since most of MOFs capture CO_2 *via* physisoprtion which leads to a lower energy investment to regenerate these materials [10]. Temperature swing adsorption (TSA) is the most common strategy for the regeneration process, nonetheless this strategy implies an extra energy consumption (heating process) [11]. One viable alternative is the pressure swing adsorption (PSA), which requires an adsorptive-adsorbent interaction of low energy and fast kinetics to compete with the TSA process. However, one of the greatest challenges of MOFs is the interaction with water molecules that can compete with gas molecules (*e.g.* CO_2) for the active sites within the pores [12,13]. To comply with the fifth and sixth

* Corresponding authors. Fax: +52 (55) 5622 4595.
E-mail addresses: kunikleto@comunidad.unam.mx (E. Sánchez-González), egz@xanum.uam.mx (E. González-Zamora), argel@unam.mx (I.A. Ibarra).

https://doi.org/10.1016/j.poly.2018.08.043
0277-5387/

criteria, the use of high-valence metal cations Cr(III), Al(III), Fe(III), V(IV), Ti(IV) and Zr(IV) has been shown to be a good strategy to achieve carboxylate-based water stable MOFs [14]. Recently, some of the most studied are the Zr-based MOFs like the UiO-66 [15], DUT-67 [16] and MOF-841 [17]. Despite their great performance and chemical stability, there is a need for the use of more earth-abundant metals in order to comply with the seventh criteria (low cost of production).

Among water stable MOFs, there is an interesting material entitled CAU-10 (CAU = Christian-Albrechts-University), an Al-based MOF with high thermal stability, competitive CO_2 uptake (10.5 wt%, 100 kPa) and certain hydrophobicity at low relative humidity (RH) [18]. The robustness of CAU-10 may be attributed to its secondary building unit (SBU), an infinite chain of [$AlO_4(OH)_2$] octahedra linked through two mutually *cis*-μ_2-OH groups (Fig. 1). This SBU combined with a 90° bent ligand, 1–3-benzenedicarboxylate, form helical chains that lead to one-dimensional square channels with free μ_2-OH groups pointing to the center of the pore in four different positions. This material shows the same topology reported for NOTT-401 [19] an Sc-based MOF, which presented exceptional robustness and adsorption properties, but it is constructed with a higher cost metal. In 2012 NOTT-300 [20], another Al-based MOF was reported with the same pore topology, but in this case the drawback was the use of a high-cost ligand BPTC (biphenyl-3,3′,5,5′-tetracarboxylic acid). Recently, Yaghi and coworkers have suggested that the presence of hydroxil functional groups within the pore structure increases the water affinity [17].

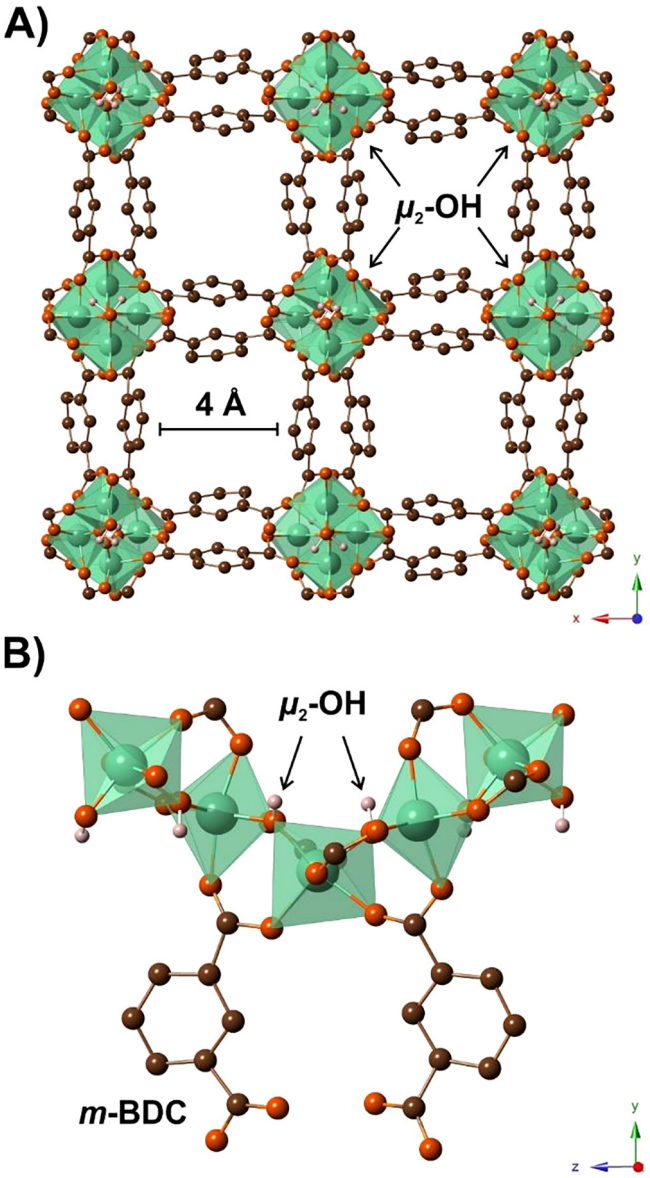

Fig. 1. CAU-10 crystal structure (A) view of the 4 Å one-dimensional channels through *c* axis; (B) infinite chain [$AlO_4(OH)_2$] octahedra SBU linked by *m*-BDC ligands through *a* axis. Atom key: Al, green; C, brown; O, orange; H, pink; ligand hydrogens were omitted.

The hydrophilicity of the pore could present a drawback in the CO_2 capture of MOFs, as previously mentioned. There are a few cases were small amounts of water within the micropores provide a positive impact on the overall CO_2 capture [21–25]. This has been showed extraordinarily by Llewelyn and coworkers in MIL-100(Fe) [26] where they demonstrate a 5-fold increase in the CO_2 uptake at 40% RH. Although, the confinement of water could provide an enhancement in the CO_2 capture, this is limited to an optimal RH value. Thus, an excess of water in the pore will decrees the material performance. To overcome this issue recently, conferring hydrophobicity to the pores has been proved to retain certain CO_2 capture under humid conditions, by simple exclusion of water from the pores [27,28]. Combining these two principles, a new CO_2 capture alternative arises, an enhancement in the total CO_2 uptake by adding a controlled amount of water, the latter dictated by the hydrophobicity of the pore.

Here we present the CO_2 adsorption under humid conditions on CAU-10, were the total capture is 1.3-fold enhanced in the lower domain of the relative humidity. This property is closely related to the hydrophobic behavior of the pore in the low RH domain, which allows a limited amount of water inside the CAU-10 channels. This confined water provides extra adsorption sites for the CO_2 uptake, resulting in the capture enhancement. PSA cycling experiments on a hydrated CAU-10 sample, corroborated a 'constant' CO_2 uptake despite the change in the pre-adsorbed water content (RH variation). The enhanced performance of CAU-10 falls in the post-combustion range of interest (5–20% RH).

2. Experimental

2.1. Materials

All reagents used were reagent grade or superior. 1-3-benzenedicarboxylic acid (*m*-H_2BDC), aluminum nitrate nonahydrated ($Al(NO_3)_3{\cdot}9H_2O$), and *N,N*-dimethylformamide (DMF) were purchased from Sigma–Aldrich and used as received without any further purification. Solvents used for washing purposes, distilled water (H_2O) and acetone (Me_2CO), were technical grade.

2.2. Synthesis

CAU-10 synthesis was modified from the reported by Stock and coworkers [18]. The aluminum salt (1.35 g, 3.6 mmol) and the 1-3-benzenedicarboxylic acid (0.6 g, 3.6 mmol) were dissolved in a H_2O:DMF mixture (4:1, 12 cm^3:3 cm^3). Synthesis was carried out in a Teflon-lined autoclave (90 cm^3) at 408 K for 12 h. Product was filtered out in a sintered-glass filter, was washed with water (5 times) and then solvent exchanged with acetone (5 times), the latter to ease the activation process. A microcrystalline white powder was isolated with an 89% yield (0.88 g).

2.3. Methods

2.3.1. General characterization

Powder X-Ray Diffraction (PXRD) patterns of the synthesized product were collected on a Bruker AXD D8 Advance diffractometer

with a Cu-Kα1 radiation (λ = 1.5406 Å). Patterns were recorded under ambient conditions in the 5-50° 2θ range with a step scan of 0.02° and a scan rate of 0.8° min^{-1}. Thermogravimetric Analysis (TGA), were performed in a Q500 HR thermobalance from TA Instruments, under N_2 atmosphere using the Hi-Res mode with a maximum rate of 5 K min^{-1} (sensitivity 1, res. 5), from room temperature to 973 K. ATR-FTIR spectra were recorded on an Alpha spectrometer from Bruker with a diamond window. Spectra were recorded from 4000 to 400 cm^{-1} with a 4 cm^{-1} resolution. N_2 isotherm at 77 K was recorded on a Belsorp mini II analyzer under high vacuum in a clean system with a diaphragm pumping system. Scanning Electron Microscopy images (SEM), were recorded using a JEOL JSM-7600F Microscope, using a lower secondary electron detector at 5 kV current in high vacuum. SEM micrographs were processed with the ImageJ software [29] for the particle size analysis.

2.3.2. Water adsorption isotherm

H_2O vapor isotherm was recorded using a dynamic method, with air as carrier gas, in a DVS Advantage 1 instrument from Surface Measurement System (mass sensitivity: 0.1 μg; Relative Humidity (RH) accuracy: 0.5% RH; vapor pressure accuracy: 0.7% P/P_0). CAU-10 sample was activated prior measurement at 453 K for 1 h under a flow of dry N_2.

2.3.3. Kinetic CO_2 adsorption experiments

Kinetic CO_2 adsorption experiments under anhydrous conditions, were performed on a Q500 HR thermobalance from TA Instruments. CAU-10 samples were activated at 453 K for 1 h under a constant N_2 flow, prior adsorption measurements. After the activation step, the samples were cooled down to 303 K, and then CO_2 uptake experiments were performed under a constant CO_2 flow of 100 cm^3 min^{-1}. Then, kinetic CO_2 adsorption at fixed RH experiments were carried out on a DVS Advantage 1 instrument from Surface Measurement System. The material was activated as described above, and then exposed to a constant RH for 1 h using N_2 as carrier gas. Afterwards, the carrier gas was changed to CO_2 (100 cm^3 min^{-1}) until equilibrium was achieved.

2.3.4. Pressure swing adsorption experiments

A pressure swing adsorption simulation was carried out on a DVS Advantage 1 instrument from Surface Measurement System. A CAU-10 sample was activated at 453 K for 1 h under a flow of dry N_2. After letting to cool down the sample to 303 K, sample was exposed to 15% P/P_0 relative humidity (40 min). Once CAU-10 sample was pre-adsorbed with water, the RH was set to zero and maintained through all the CO_2 adsorption–desorption cycles. Immediately after a constant CO_2 flow (100 cm^3 min^{-1}) was set for 20 min for the adsorption step, then CO_2 flow was set to zero for the desorption step for other 20 min to complete each cycle (no other gas was used to purged out the CO_2). Additionally, the same cycling was performed with an anhydrous CAU-10.

3. Results and discussion

The CAU-10 structure was corroborated by the PXRD profile refinement (Fig. 2), using the Le Bail Method (FullProf software) [30,31]. The thermogravimetrical analysis showed a 22% mass loss at 320 K, which corresponded with occluded water molecules; at 650 K began the decomposition of the material with a 55.5% mass loss (Fig. S1). The CAU-10 acetone exchanged sample was used to ease the activation process and assure a fully desolvated sample. The N_2 isotherm exhibited a type I isotherm, correspondent to microporous materials (Fig. S4). The estimated surface area of CAU-10 was 615 m^2 g^{-1}, which agrees with the reported value

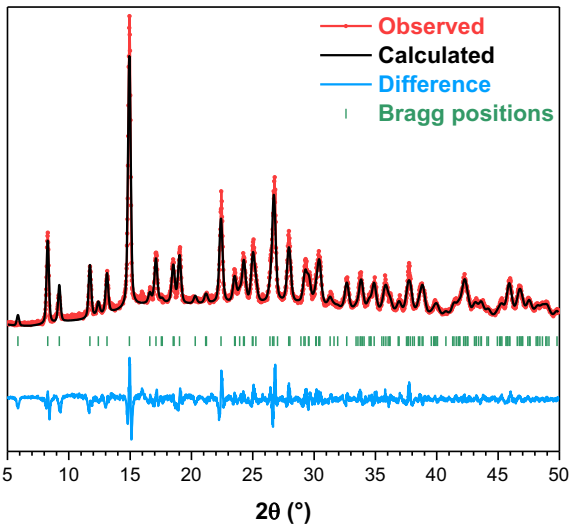

Fig. 2. Le Bail fit of the PXRD pattern of CAU-10 as synthesized.

(635 m^2 g^{-1}) [18]. This basic characterization showed the reproducibility of the material.

Water adsorption experiment at 303 K on the CAU-10 sample showed a s-shaped isotherm (Fig. 3). The water adsorption was slow from 0 to 15% P/P_0 with a 1.1 wt% uptake, in this relative humidity domain behaves as a hydrophobic material. Then, at 20% P/P_0 the material presents a steep increase in the water uptake to reach a saturation of 28.8 wt% at 40% P/P_0, as a hydrophilic material (Fig. 3). From this point onwards, a small increase in the water uptake leads to a 33.2 wt% total uptake. The desorption presents a broad hysteresis, the material began to desorb at 20% P/P_0. For hydrophilic materials, when the RH is increased the water content should increase accordingly until a saturation point. Whereas for a hydrophobic material, the water content will be constant regardless the increment of the RH. This is also true for a bifunctional material before the adsorption trigger point (hydrophobic behavior), after which the material rapidly adsorbs water (hydrophilic behavior) (Fig. S5). CAU-10 exhibits this bifunctional behavior (Fig. 3), and its adsorption trigger point (20% P/P_0) is above the range of RH in a post combustion flue [10]. This suggest that CAU-10 could behave as a hydrophobic material in these industrial relevant conditions.

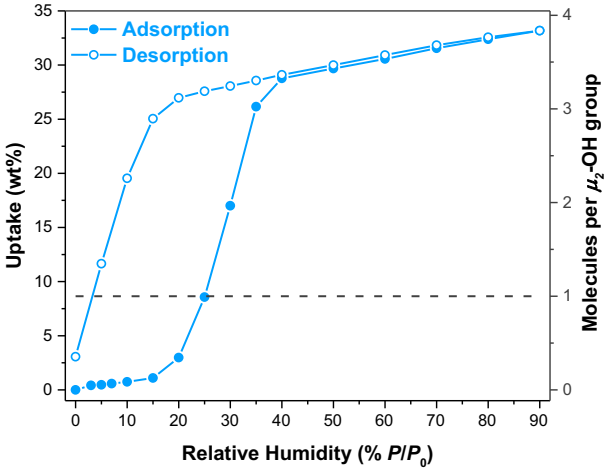

Fig. 3. CAU-10 water adsorption isotherm at 303 K, gravimetric uptake comparison with adsorption sites occupancy.

Farrusseng and coworkers, used the Henry's constant (K_H) and an α parameter (the half saturation P/P_0) to determine the hydrophobicity of a MOF [32]. There, the authors associate low K_H and high α values to hydrophobic MOFs. Another microporous Al-based MOF was tested, MIL-53(Al) presented a $K_H = 1.17 \cdot 10^{-6}$ mol g^{-1} Pa^{-1} and $\alpha = 0.14$. For the CAU-10 we found a $K_H = 6.18 \cdot 10^{-7}$ mol g^{-1} Pa^{-1} and $\alpha = 0.3$ (Fig. S6), these values demonstrate a higher hydrophobicity for the CAU-10. The parameters K_H and α are associated with the surface chemistry and pore size respectively. CAU-10 as MIL-53(Al) channels are decorated with hydroxo groups, thus the surface of their pores is not that different, the main difference are their pore sizes 7–13 Å for MIL-53(Al) and 4 Å for CAU-10. The value of α for CUA-10 is greater than MIL-53(Al), associated with a reduced pore size therefore its higher degree of hydrophobicity.

A closer look into the pore filling reveals another interesting aspect of CAU-10. In the low relative humidity domain, values below 15% RH, only 1 of every 10 μ_2-OH groups has a water molecule adsorbed (Fig. 3), this leaves other 9 potential adsorption sites for other molecules to be occupied (*e.g.* CO_2). Surface area measurement of a hydrated CAU-10 sample (15% RH), corroborated that 90% of the original surface area remained accessible (556 of 615 m^2 g^{-1}, Fig. S4). It is worth noticed that this RH domain falls within the range of water content of typical postcombustion flue gas composition (5–15% RH) [10]. Thus, we evaluated the CAU-10 CO_2 capture under dynamic conditions.

Kinetic CO_2 capture experiments on the CAU-10 were performed first under anhydrous conditions at 303 K. A sample was activated, prior measurements, at 453 K with a N_2 flow (*vide supra*), after the sample cooled down to 303 K a continuous CO_2 flow was applied to the sample. The CAU-10 presented a relatively fast adsorption reaching saturation, 5.43 wt%, in only 10 min (Fig. 4A). In the same fashion, the desorption step took 15 min to be completed without applying any heat (Fig. S7).

Kinetic CO_2 capture experiments under fixed relative humidity at 303 K, were carried on CAU-10 in the industrial relevant range (3–25% P/P_0). The samples were activated before each measurement (*vide supra*), then a sample was exposed to a constant relative humidity (5% P/P_0 Fig. 4B blue line). The water saturation step took 50 min, considerably higher than the CO_2 (10 min), this may be attributed to a strong water H-bond interaction with the μ_2-OH groups. After the water uptake reached a plateau 0.54 wt% (90 min), carrier gas was set to CO_2 maintaining the RH at 5% P/P_0 (Fig. 4B). The uptake began with a pronounced steep, but equilibrium took 30 min to reach saturation with 7.26 wt% of total CO_2 uptake (Fig. 4B red line), this value was taken from the total uptake minus the pre-adsorbed water. Surprisingly, the total uptake showed a 1.3-fold increase, respect to the anhydrous condition (from 5.43 to 7.26 wt%), albeit there are 0.54 wt% water inside the pore.

Furthermore, this increment in the total CO_2 adsorption can be explained by the augment in the adsorption sites. At lower water loadings, the water molecules can be regularly distributed inside the pore through hydrogen bonds with the μ_2-OH groups [33,34]. This anchored water molecules provide an extra adsorption site where the CO_2 can interact. Same effect has been observed in other microporous μ_2-OH containing MOFs (Fig. 5). The materials presented in Fig. 5 have the same type of one-dimensional channel and the $[MO_4(OH)_2]$ octahedra chain SBU, with exception of MIL-53(Al) which exhibits *trans*-μ_2-OH groups in the SBU that confers to this one the 'soft crystalline' property. From this set of data, we can notice that even though the CAU-10 has half the surface are of the other materials, it presents the higher CO_2 uptake under anhydrous and at low RH conditions. The CO_2 with a kinetic diameter of 3.3 Å, is more efficiently packed inside the narrow pores of CAU-10 (4 Å). This reduction of the pore strategy to enhance the CO_2 uptake has been proved in the SIFSIX family [35].

Taking a look into the CO_2 uptake values obtained in the range of 3–20% P/P_0, we can observe a constant capture in this range (Fig. 6 circles). When the RH is increased to 25% P/P_0, no CO_2 capture is observed since the adsorption sites are already occupied by water. We can hypothesize that the water content of the pore is directly regulating this CO_2 enhancement. Since there is not the exactly same amount of water in each experiment a slightly decrease in the CO_2 uptake is observed with the increase of RH within this range. Remarkably, the CAU-10 hydrophobic domain (3–20% P/P_0) maintains the right amount of water to enhance the CO_2 adsorption almost constant. Despite a lot of work has been done in the humidity controllers and adsorption driven heat pumps [36–38], this 'self-regulated' water content has not been explored for CO_2 capture applications at low RH conditions. Typically, the adsorbents with high CO_2 uptake requires an optimum RH value for a CO_2 uptake enhancement (Fig. S8), which could limit their performance in real-life conditions.

After reviewing the CO_2 capture properties of CAU-10 at different RH values, it is pertinent to know the absorption kinetics as the

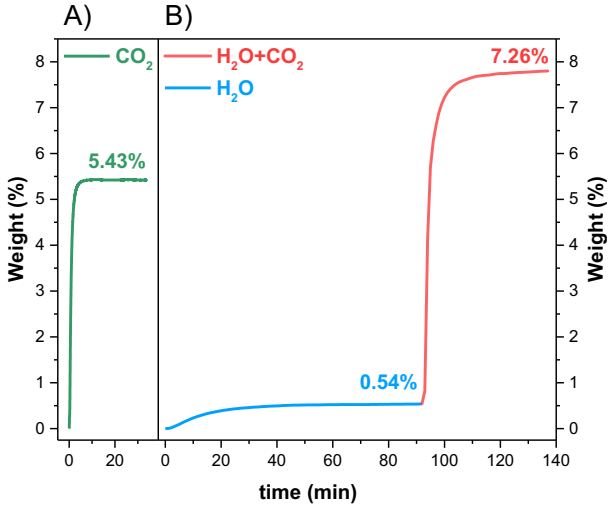

Fig. 4. Kinetic CO_2 adsorption experiments at 303 K, (A) anhydrous conditions and (B) at fixed Relative Humidity (5% P/P_0).

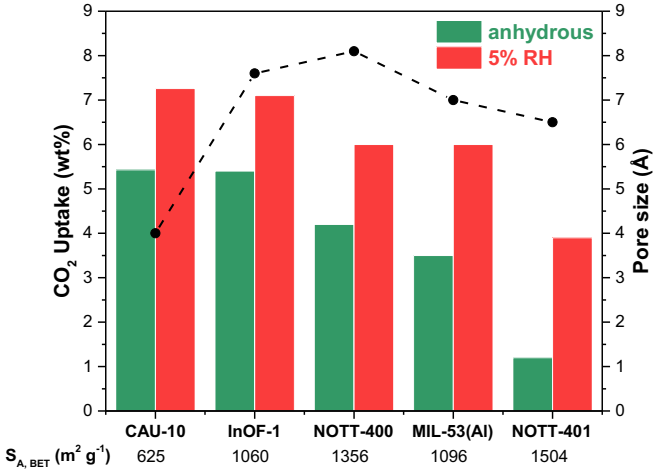

Fig. 5. Comparison of kinetic CO_2 uptake for CAU-10 and related microporous MOFs: InOF-1 [21], NOTT-400 [22], MIL-53(Al) [25] and NOTT-401 [24]. CO_2 uptake in anhydrous conditions (green bars) and at 5% RH (red bars), pore size (black circles), and BET surface area values (values below *x* axis).

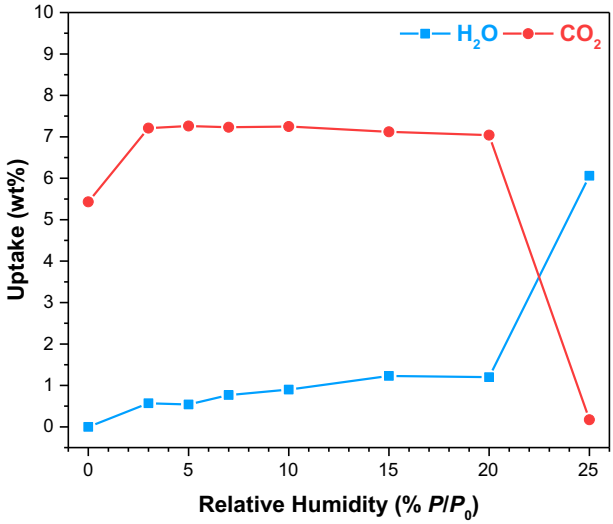

Fig. 6. CAU-10 individual uptake of pre-adsorbed H_2O (squares) and CO_2 capture (circles) for different Relative Humidity values at 303 K.

second criteria of the ideal adsorbent dictates. As mentioned earlier, a drastic increase in the equilibrium time for the CO_2 uptake at imposed RH was observed. This was corroborated by comparing the CO_2 diffusion coefficients (D_M) (See Supplementary Data), for the anhydrous condition $4.13 \cdot 10^{-8}$ cm^2 s^{-1}, which is almost the double of the value at 5% RH ($1.94 \cdot 10^{-8}$ cm^2 s^{-1}). The reduction of the adsorption velocity can be attributed to hydrogen bond interactions between the pre-adsorbed water and the CO_2 molecules. The diffusion activation energy (E_a) was estimated form kinetic CO_2 adsorption experiments at different temperatures (303–323 K). Thus, these CO_2 E_a values for CAU-10 were obtained by means of the Arrhenius equation [39], 6.87 and 19.63 kJ mol^{-1} for the anhydrous and 5% RH respectively (Fig. S15). The diffusion activation energy in the presence of relative humidity confirms the interaction of the CO_2 molecules with the water molecules within the pores, implying an extra time for material regeneration in a PSA regime. Additionally, the effect of the relative humidity in the diffusion of CO_2 was investigated on CAU-10. As suspected from the kinetic adsorption experiments, the diffusion coefficient remains almost the same in the range of 3–20% P/P_0 (Fig. 7). This

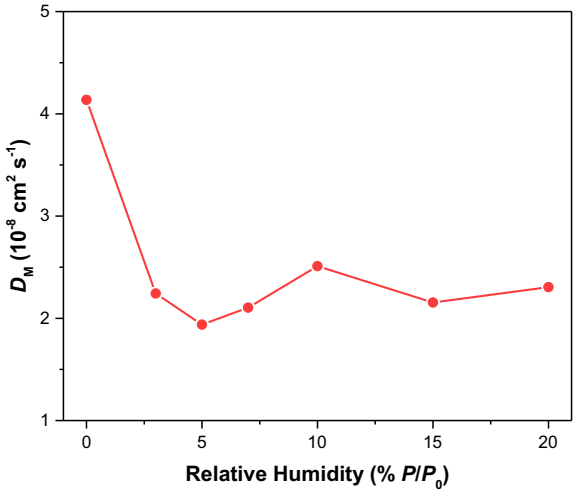

Fig. 7. Diffusivity coefficient of CO_2 on CAU-10 for different Relative Humidity values at 303 K.

kinetic feature, ensures a fixed adsorption and/or desorption time despite the RH value (within this range). Thus, CAU-10 regeneration times will not change upon different operating conditions, adsorbing-desorbing the same amount of CO_2 regardless the relative humidity (in the low RH domain).

Finally, pressure swing adsorption cycles were performed on a hydrated CAU-10 sample. A CAU-10 activated sample was exposed to a constant RH 15% P/P_0, after reaching equilibrium (1 wt% H_2O uptake) RH was set to 0% P/P_0 and immediately exposed to a constant CO_2 flow (100 cm^3 min^{-1}). After 20 min of CO_2 adsorption (7.11 wt% CO_2 uptake), the CO_2 flow was set to zero to simulate a PSA cycle (Fig. 8A). Another five cycles were performed on the same sample, were the CAU-10 demonstrated a reversible CO_2 uptake of 7.02 ± 0.04 wt% despite the decrease in the water content (Fig. 8B). A shift in the baseline is observed due to the loss of the pre-adsorbed water upon each cycle (from 1 to 0.2 wt%), this demonstrate that a small change in the content of water does not affect the CO_2 adsorption. Remarkably, the desorption step did not require temperature to completely released the adsorbed CO_2. This feature agrees with the fourth criteria of an ideal adsorbent (mild regeneration conditions). Also, the structure stability was corroborated by PXRD after the CO_2 adsorption–desorption cycles with H_2O (Fig. S17), demonstrating that the fifth criteria was also met (stability during adsorption–desorption cycling).

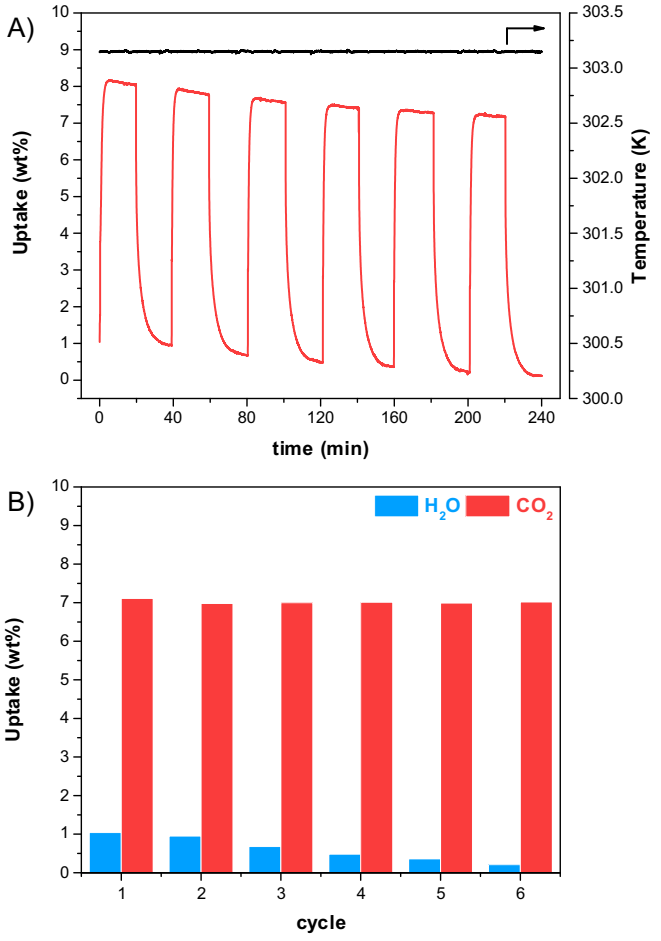

Fig. 8. CO_2 adsorption–desorption cycling for hydrated CAU-10, (A) PSA cycles (red trace) at constant temperature (black trace) and (B) individual uptake of pre-adsorbed H_2O and CO_2 capture at each cycle. Prior measurements an CAU-10 activated sample was exposed to 15% RH for 40 min to pre-adsorb the water. Cycles were performed at 0% RH, with a CO_2 flow of 100 and zero cm^3 min^{-1} for the adsorption and desorption steps.

Recapitulating, CAU-10 proves to be a good adsorbent because it complies with most of the seven fundamental criteria for an ideal adsorbent:

I. High CO_2 adsorption capacity: 5.4 wt% under anhydrous conditions and it was increased to 7.3 wt% at 5% RH (303 K).
II. Fast adsorption kinetics: D_M value of $1.94 \cdot 10^{-8}$ cm^2 s^{-1} for CO_2 at 5% RH (303 K).
III. High CO_2 selectivity: although was not formally proved, before the CO_2 capture experiments the water pre-adsorption step was carried out with N_2. Then, a rather good selectivity is assumed since a clear increase in the mass is observed upon CO_2 exposure.
IV. Mild regeneration conditions: CAU-10 regeneration was achieved in a pressure swing adsorption regime, without the need to apply additional heat.
V. Stability during adsorption–desorption cycling: crystallinity was remained after the cycling, it was confirmed with PXRD.
VI. Stability towards moisture: CAU-10 is a water stable material.
VII. Low cost of production: aluminum is one of the cheapest metals and also the 1-3-benzenedicarboxylic acid is a low-cost ligand.

4. Conclusions

CO_2 uptake of CAU-10 was tested in a range of industrial relevant humid conditions. Due to the pore hydrophobic nature, it is possible to maintain the 'same' amount of water over at low RH conditions (3–20% P/P_0). Taking advantage of this water inside the pore, we demonstrated a 1.3-fold CO_2 enhancement in the whole range of RH (3–20% P/P_0). This confinement effect presents a 'constant' CO_2 uptake and diffusion coefficient, albeit the variation in the RH. This 'constant' CO_2 capture enhancement, was demonstrated with adsorption–desorption cycles in a hydrated CAU-10 sample under a PSA regime. These properties set a precedent to design that ideal CO_2 adsorbent for postcombustion effluents and launch CAU-10 as a potential CO_2 adsorbent at industrial level.

Acknowledgements

The authors thank A. Yañez-Aulestia for the aid with the SEM micrographs. Financial support for this work was provided by PAPIIT UNAM Mexico (IN101517), CONACyT Mexico under grant Nos. 1789 (I.A.I.), 236879 (E.G.-Z.) and 289042 (E.S.-G.).

Appendix A. Supplementary data

Supplementary data associated with this article can be found, in the online version, at https://doi.org/10.1016/j.poly.2018.08.043.

References

[1] L. Barrie, G. Braathen, WMO GREENHOUSE GAS BULLETIN The State of Greenhouse Gases in the Atmosphere Based on Global Observations through 2016, (n.d.).
[2] R.A. Betts, C.D. Jones, J.R. Knight, R.F. Keeling, J.J. Kennedy, El Niño and a record CO2 rise, Nat. Clim. Chang. 6 (2016) 806, https://doi.org/10.1038/nclimate3063.
[3] D.S. Sholl, R.P. Lively, Seven chemical separations to change the world, Nature 532 (2016) 435, https://doi.org/10.1038/532435a.
[4] A. Sayari, Y. Belmabkhout, R. Serna-Guerrero, Flue gas treatment via CO2 adsorption, Chem. Eng. J. 171 (2011) 760, https://doi.org/10.1016/J.CEJ.2011.02.007.
[5] S. Nanda, S.N. Reddy, S.K. Mitra, J.A. Kozinski, The progressive routes for carbon capture and sequestration, Energy Sci. Eng. 4 (2016) 99, https://doi.org/10.1002/ese3.117.
[6] G. Férey, Microporous solids: from organically templated inorganic skeletons to hybrid frameworks. Ecumenism in chemistry, Chem. Mater. 13 (2001) 3084, https://doi.org/10.1021/cm011070n.
[7] J.L.C. Rowsell, O.M. Yaghi, Metal–organic frameworks: a new class of porous materials, Microporous Mesoporous Mater. 73 (2004) 3–14, https://doi.org/10.1016/J.MICROMESO.2004.03.034.
[8] C. Janiak, J.K. Vieth, MOFs, MILs and more: concepts, properties and applications for porous coordination networks (PCNs), New J. Chem. 34 (2010) 2366–2684, https://doi.org/10.1039/c0nj00275e.
[9] A. Das, D.M. D'Alessandro, Tuning the functional sites in Metal-Organic Frameworks to modulate CO_2 heats of adsorption, CrystEngComm 17 (2015) 706–718, https://doi.org/10.1039/C4CE01341G.
[10] K. Sumida, D.L. Rogow, J.A. Mason, T.M. McDonald, E.D. Bloch, Z.R. Herm, T.-H. Bae, J.R. Long, Carbon dioxide capture in metal organic frameworks, Chem. Rev. 112 (2012) 724–781, https://doi.org/10.1021/cr2003272.
[11] J.A. Mason, K. Sumida, Z.R. Herm, R. Krishna, J.R. Long, Evaluating metal–organic frameworks for post-combustion carbon dioxide capture via temperature swing adsorption, Energy Environ. Sci. 4 (2011) 3030, https://doi.org/10.1039/c1ee01720a.
[12] E. González-Zamora, I.A. Ibarra, CO2 capture under humid conditions in metal–organic frameworks, Mater. Chem. Front. 1 (2017) 1471, https://doi.org/10.1039/C6QM00301J.
[13] J. Canivet, A. Fateeva, Y. Guo, B. Coasne, D. Farrusseng, Water adsorption in MOFs: fundamentals and applications, Chem. Soc. Rev. 43 (2014) 5594, https://doi.org/10.1039/C4CS00078A.
[14] A.J. Howarth, Y. Liu, P. Li, Z. Li, T.C. Wang, J.T. Hupp, O.K. Farha, Chemical, thermal and mechanical stabilities of metal–organic frameworks, Nat. Rev. Mater. 1 (2016) 15018, https://doi.org/10.1038/natrevmats.2015.18.
[15] J.H. Cavka, S. Jakobsen, U. Olsbye, N. Guillou, C. Lamberti, S. Bordiga, K.P. Lillerud, A new zirconium inorganic building brick forming metal organic frameworks with exceptional stability, J. Am. Chem. Soc. 130 (2008) 13850, https://doi.org/10.1021/ja8057953.
[16] V. Bon, I. Senkovska, I.A. Baburin, S. Kaskel, Zr- and Hf-based metal–organic frameworks: tracking down the polymorphism, Cryst. Growth Des. 13 (2013) 1231, https://doi.org/10.1021/cg301691d.
[17] H. Furukawa, F. Gándara, Y.-B. Zhang, J. Jiang, W.L. Queen, M.R. Hudson, O.M. Yaghi, Water adsorption in porous metal-organic frameworks and related materials, J. Am. Chem. Soc. 136 (2014) 4369, https://doi.org/10.1021/ja500330a.
[18] H. Reinsch, M.A. van der Veen, B. Gil, B. Marszalek, T. Verbiest, D. de Vos, N. Stock, Structures, sorption characteristics, and nonlinear optical properties of a new series of highly stable aluminum MOFs, Chem. Mater. 25 (2013) 17–26, https://doi.org/10.1021/cm3025445.
[19] I.A. Ibarra, S. Yang, X. Lin, A.J. Blake, P.J. Rizkallah, H. Nowell, D.R. Allan, N.R. Champness, P. Hubberstey, M. Schröder, Highly porous and robust scandium-based metal–organic frameworks for hydrogen storage, Chem. Commun. 47 (2011) 8304, https://doi.org/10.1039/c1cc11168j.
[20] S. Yang, J. Sun, A.J. Ramirez-Cuesta, S.K. Callear, W.I.F. David, D.P. Anderson, R. Newby, A.J. Blake, J.E. Parker, C.C. Tang, M. Schröder, Selectivity and direct visualization of carbon dioxide and sulfur dioxide in a decorated porous host, Nat. Chem. 4 (2012) 887, https://doi.org/10.1038/nchem.1457.
[21] R.A. Peralta, B. Alcántar-Vázquez, M. Sánchez-Serratos, E. González-Zamora, I. A. Ibarra, Carbon dioxide capture in the presence of water vapour in InOF-1, Inorg. Chem. Front. 2 (2015) 898–903, https://doi.org/10.1039/C5QI00077G.
[22] J.R. Álvarez, R.A. Peralta, J. Balmaseda, E. González-Zamora, I.A. Ibarra, Water adsorption properties of a Sc(III) porous coordination polymer for CO2 capture applications, Inorg. Chem. Front. 2 (2015) 1080–1084, https://doi.org/10.1039/C5QI00176E.
[23] M. Sánchez-Serratos, P.A. Bayliss, R.A. Peralta, E. González-Zamora, E. Lima, I.A. Ibarra, CO2 capture in the presence of water vapour in MIL-53(Al), New J. Chem. 40 (2016) 68, https://doi.org/10.1039/C5NJ02312B.
[24] E. Sánchez-González, J.R. Álvarez, R.A. Peralta, A. Campos-Reales-Pineda, A. Tejeda-Cruz, E. Lima, J. Balmaseda, E. González-Zamora, I.A. Ibarra, Water adsorption properties of NOTT-401 and CO2 capture under humid conditions, ACS Omega 1 (2016) 305, https://doi.org/10.1021/acsomega.6b00102.
[25] A. Zárate, R.A. Peralta, P.A. Bayliss, R. Howie, M. Sánchez-Serratos, P. Carmona-Monroy, D. Solis-Ibarra, E. González-Zamora, I.A. Ibarra, CO2 capture under humid conditions in NH2 -MIL-53(Al): the influence of the amine functional group, RSC Adv. 6 (2016) 9978–9983, https://doi.org/10.1039/C5RA26517G.
[26] E. Soubeyrand-Lenoir, C. Vagner, J.W. Yoon, P. Bazin, F. Ragon, Y.K. Hwang, C. Serre, J.S. Chang, P.L. Llewellyn, How water fosters a remarkable 5-fold increase in low-pressure CO 2 uptake within mesoporous MIL-100(Fe), J. Am. Chem. Soc. 134 (2012) 10174, https://doi.org/10.1021/ja302787x.
[27] N.T.T. Nguyen, H. Furukawa, F. Gándara, H.T. Nguyen, K.E. Cordova, O.M. Yaghi, Selective capture of carbon dioxide under humid conditions by hydrophobic chabazite-type zeolitic imidazolate frameworks, Angew. Chem. Int. Ed. 53 (2014) 10645, https://doi.org/10.1002/anie.201403980.
[28] C.A. Trickett, A. Helal, B.A. Al-Maythalony, Z.H. Yamani, K.E. Cordova, O.M. Yaghi, The chemistry of metal–organic frameworks for CO2 capture, regeneration and conversion, Nat. Rev. Mater. 2 (2017) 17045, https://doi.org/10.1038/natrevmats.2017.45.
[29] W. Rasband, ImageJ software, 2015.
[30] Y. Laligant, A. Le Bail, F. Goutenoire, Ab initio structure determination of lanthanum cyclo-tetratungstate α-La2W2O9 from X-ray and neutron powder diffraction, J. Solid State Chem. 159 (2001) 223, https://doi.org/10.1006/JSSC.2001.9189.

[31] T. Riosnel, J. Gonzalez-Platas, J. Rodriguez-Carvajal, FullProf suite program, 2015.
[32] J. Canivet, J. Bonnefoy, C. Daniel, A. Legrand, B. Coasne, D. Farrusseng, Structure–property relationships of water adsorption in metal–organic frameworks, New J. Chem. 38 (2014) 3102, https://doi.org/10.1039/C4NJ00076E.
[33] F. Salles, S. Bourrelly, H. Jobic, T. Devic, V. Guillerm, P. Llewellyn, C. Serre, G. Ferey, G. Maurin, Molecular insight into the adsorption and diffusion of water in the versatile hydrophilic/hydrophobic flexible MIL-53(Cr) MOF, J. Phys. Chem. C. 115 (2011) 10764, https://doi.org/10.1021/jp202147m.
[34] V. Haigis, F.-X. Coudert, R. Vuilleumier, A. Boutin, Investigation of structure and dynamics of the hydrated metal-organic framework MIL-53(Cr) using first-principles molecular dynamics, Phys. Chem. Chem. Phys. 15 (2013) 19049, https://doi.org/10.1039/c3cp53126k.
[35] P. Nugent, Y. Belmabkhout, S.D. Burd, A.J. Cairns, R. Luebke, K. Forrest, T. Pham, S. Ma, B. Space, L. Wojtas, M. Eddaoudi, M.J. Zaworotko, Porous materials with optimal adsorption thermodynamics and kinetics for CO2 separation, Nature 495 (2013) 80–84, https://doi.org/10.1038/nature11893.
[36] D. Fröhlich, S.K. Henninger, C. Janiak, Multicycle water vapour stability of microporous breathing MOF aluminium isophthalate CAU-10-H, Dalt. Trans. 43 (2014) 15300–15304, https://doi.org/10.1039/C4DT02264E.
[37] M.F. de Lange, T. Zeng, T.J.H. Vlugt, J. Gascon, F. Kapteijn, Manufacture of dense CAU-10-H coatings for application in adsorption driven heat pumps: optimization and characterization, CrystEngComm 17 (2015) 5911–5920, https://doi.org/10.1039/C5CE00789E.
[38] D. Lenzen, P. Bendix, H. Reinsch, D. Fröhlich, H. Kummer, M. Möllers, P.P.C. Hügenell, R. Gläser, S. Henninger, N. Stock, Scalable green synthesis and full-scale test of the metal-organic framework CAU-10-H for use in adsorption-driven chillers, Adv. Mater. 30 (2018) 1705869, https://doi.org/10.1002/adma.201705869.
[39] Z. Zhao, Z. Li, Y.S. Lin, Adsorption and diffusion of carbon dioxide on metal−organic framework (MOF-5), Ind. Eng. Chem. Res. 48 (2009) 10015, https://doi.org/10.1021/ie900665f.